Mathematical Modelling and Control

http://www.aimspress.com/journal/mmc

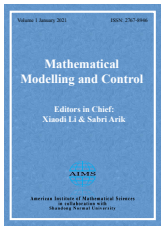

MMC, 5(2): 147–163.
DOI: 10.3934/mmc.2025011
Received: 18 September 2024
Revised: 23 November 2024
Accepted: 09 December 2024
Published: 21 May 2025

Research article

Efficient numerical method for pricing multi-asset options with the time-fractional Black-Scholes model: focus on American and digital options

Imtiaz Ahmad[1,2,*], **Muhammad Nawaz Khan**[3,*], **Rashid Jan**[4,5] **and Normy Norfiza Abdul Razak**[5]

[1] Institute of Informatics and Computing in Energy (IICE), Universiti Tenaga Nasional, Kajang, Selangor, Malaysia

[2] Department of Mathematics, Saveetha School of Engineering (SIMATS), Thandalam 600124, Chennai, Tamil Nadu, India

[3] Mathematics in Applied Sciences and Engineering Research Group, Scientific Research Center, Al-Ayen University, Nasiriyah 64001, Iraq

[4] Department of Mathematics, Khazar University AZ1096, Baku, Azerbaijan

[5] Institute of Energy Infrastructure (IEI), Department of Civil Engineering, College of Engineering, Universiti Tenaga Nasional (UNITEN), Putrajaya Campus, Jalan IKRAM-UNITEN, 43000 Kajang, Selangor, Malaysia

* **Correspondence:** Email: imtiazkakakhil@gmail.com, mnawaz77@gmail.com.

Abstract: This study presents a numerical solution for the two-asset time-fractional Black-Scholes model, which governs American and digital options, using a local meshless collocation method based on Gaussian radial basis functions. The proposed meshless approach effectively discretized the spatial derivatives of the model, while the Caputo derivative was employed to represent the time-fractional component, capturing the memory effects and non-local properties characteristic of fractional-order models. Numerical assessments were conducted to evaluate the method's performance across these option models. The study discusses the handling of interest rates, highlighting the method's capability to manage the complexities inherent in multi-asset options. The efficacy and accuracy of the proposed meshless approach were evaluated using the L_∞ error norms. In the absence of exact solutions for these option models, the double mesh technique was utilized to validate the accuracy and efficiency of the proposed method, ensuring the robustness and reliability of the numerical results.

Keywords: meshless method; American and digital options; Caputo derivative; gaussian radial function; numerical analysis

1. Introduction

Fractional calculus, which extends classical calculus to include derivatives and integrals of non-integer orders, has emerged as a significant tool in the domain of financial derivatives and investment, particularly for the pricing of stock options [1, 2]. This advanced approach effectively addresses the complex, non-local effects prevalent in financial markets that traditional models often inadequately capture. By integrating fractional derivatives, fractional calculus provides a more detailed representation of market dynamics and price movements. In the context of stock options and financial models [3], fractional calculus can detect atypical behaviors and volatility clustering that may be overlooked by conventional models [4]. This enhances the accuracy of pricing and risk assessment, enabling investors to better hedge against potential market disruptions. The application of fractional calculus in option pricing models offers a sophisticated alternative to traditional methods, aligning more closely with the

empirical observations of financial markets, where one of the most essential elements in financial derivatives and investing is the stock option. The study of partial differential equation (PDE) models for option pricing is crucial and should be extended beyond integer order, both theoretically and practically. Black and Scholes [5] developed a model for stock price and time using second-order parabolic integer-order PDEs, depending on geometric Brownian motion with volatility and continuous drift. However, integer-order PDEs may fail to capture the significant volatility of a stock price accurately, especially in scenarios involving jumps over tiny time steps, due to the assumptions of the Black-Scholes model [6]. To better understand market dynamics, current research has explored extending the Black-Scholes model using fractional calculus. For instance, Alaje et al. [7] applied a modified homotopy perturbation approach to solve Caputo fractional-order Black-Scholes equations, while Ogunyebi et al. [8] provided a direct solution for non-integer order Black-Scholes models. Their results indicated that fractional-order derivatives offer greater flexibility in modeling option pricing. The fractional Taylor formula was employed by Jumarie [9] to construct the fractional Black-Scholes models. Korbel & Luchko [10] introduced a space-time fractional diffusion equation with changing order that preserves global scaling features and permits intricate short-term behavior. Farhadi et al. [11] introduced a time-fractional version to capture trend memory. A fractional diffusion model was created by the authors of [12] to price exotic options in markets that are undergoing jumps. Li et al. [13] developed a fractional stochastic differential equation model that includes trend memory in option pricing, finding it to be more accurate than traditional models. These studies underscore the potential of fractional calculus in financial modeling, offering more nuanced representations of market behavior and memory effects in option pricing. In Chen [14], the fractional Black-Scholes model incorporating the American option was addressed using a predictor-corrector scheme. Moreover, Chen and Wang [15] investigated a space-fractional parabolic variational inequality model for pricing American options by integrating a finite-difference scheme with a power penalty strategy. Further research in this area is particularly important and beneficial, given the increasing challenges in solving increasingly complex fractional BS partial differential equation models.

Two-asset options are actively traded in various financial markets, including fixed income, equity, foreign exchange, and commodities, both on organized exchanges and over-the-counter. For pricing two-dimensional options in discrete settings, several transformation methods have been proposed, such as the Shannon wavelet inverse Fourier method [16] and the Fourier cosine method [17, 18]. The distinctive qualities of fractional operators have led to increasing recognition of the application of fractional calculus in option pricing [19–21]. Most existing research has concentrated on single-asset option pricing within the framework of fractional PDEs, which motivates the goal of this paper to extend these methods to two-asset option pricing. Kim [22] used the finite difference method to solve multi-asset Black-Scholes equations, offering a detailed implementation strategy and evaluating its accuracy and efficiency for complex option pricing. Vcerna [23] used orthogonal spline wavelets and focused on a multifactor Black-Scholes model, improving computational efficiency and accuracy in pricing options with multiple factors. Choi [24] integrated various Black-Scholes-Merton models to create a unified pricing method for complex instruments like spread, basket, and Asian options, aiming to boost both pricing accuracy and efficiency. Bayer [25] applied Quasi-Monte Carlo procedures to Fourier-based pricing for multi-asset options, using quasi-random sequences to enhance accuracy and reduce computational costs, and showcasing advantages over traditional Monte Carlo procedures. For the two-dimensional fractional Black-Scholes (FBS) equation, the authors in [26] proposed a second-order finite difference technique, which Chen and Wang [27] applied to price two assets American options. However, it becomes computationally costly to solve the linear systems obtained from the discretization of two- or higher-dimensional FBS equations due to the ensuing dense coefficient matrices. In the options market, prolonged computation times can negatively impact pricing accuracy, making the results less reliable. Therefore, improving computational efficiency is essential for overcoming the challenges of multi-dimensional FBS equations and for practical application in option pricing.

The multi-asset Black-Scholes PDE model's generic form is provided as

$$\frac{\partial^{\alpha} P}{\partial \tau^{\alpha}} + \Omega P(\overline{\mathbf{y}}, \tau) = 0, \qquad \tau < T, \quad \overline{\mathbf{y}} \in \mathbf{R}_{+}^{n}, \tag{1.1}$$

where

$$\begin{aligned}\Omega P(\overline{\mathbf{y}}, \tau) =& \frac{1}{2}\sigma_1^2 y^2 \frac{\partial^2 P}{\partial y^2} + \frac{1}{2}\sigma_2^2 z^2 \frac{\partial^2 P}{\partial z^2} + \frac{1}{2}\rho\sigma_1\sigma_2 yz \frac{\partial^2 P}{\partial y \partial z} \\ &+ (r - D_1) y \frac{\partial P}{\partial y} + (r - D_2) z \frac{\partial P}{\partial z} - rP.\end{aligned} \tag{1.2}$$

In this context, the following variables are used to represent key financial parameters: $\overline{\mathbf{y}}$ denotes the prices of the underlying assets, D_i is the dividend yield for the ith asset, r is the risk-free interest rate, σ_i represents the volatility of the ith underlying asset, and ρ_{ij} indicates the correlation between the ith and jth assets where $i, j = 1, 2$. Additionally, n signifies the spatial dimension, and the price of the underlying asset $\overline{\mathbf{y}}$ functions as a spatial variable within the problem.

The option value, denoted as $P(\overline{\mathbf{y}}, \tau)$ before the expiration time T, can be transformed into an initial value problem by applying the change of variable $t = T - \tau$. This transformation simplifies the final value problem presented in Eq (1.1).

Recent developments in numerical methods have significantly improved the solutions for linear, nonlinear, and time-fractional partial differential equations [28–34]. Among these innovations, meshless methods have become particularly notable. In particular, methods employing RBFs are recognized as an effective approach for solving a wide range of PDEs, including those involving fractional derivatives. The advantages of RBF-based methods include their adaptability to higher-dimensional and irregular domains [35, 36]. These techniques have demonstrated success in addressing both linear and nonlinear fractional PDEs, including time-fractional convective-diffusion and wave equations, and fractional Fisher's equations [37, 38]. Additionally, RBF-based methods have been extended to handle three-dimensional multi-term time-fractional PDEs [39]. They have also proven effective for solving intricate nonlinear PDE systems, including Drinefel'd-Sokolov-Wilson equations, and the Hirota-Satsuma coupled KdV system [40, 41]. These findings illustrate that RBF-based meshless methods provide a valuable alternative to conventional numerical approaches for addressing complex PDEs in various scientific and engineering applications.

Meshless methods can be categorized into local as well as global approaches. While using global interpolation, the global meshless method (GMM) faces challenges such as the production of ill-conditioned, dense matrices and the shape parameter sensitivity. To overcome these issues, researchers have introduced a local meshless method (LRBFM) that utilizes local interpolation within sub-domains [38, 42]. LRBFM have emerged as an alternative to GMMs for solving PDEs. LRBFM provide benefits such as reduced sensitivity to shape parameter variations and enhanced computational efficiency by working with smaller matrices [42]. These methods have been effectively applied to various PDEs [42, 43]. LRBFM exhibit flexibility in managing both regular and irregular domains, with the ability to handle uniform and scattered nodal points [44]. Comparative studies indicate that local meshless methods offer similar accuracy to GMMs while providing greater stability, particularly with larger node counts. The local approach also facilitates easier implementation and achieves higher convergence rates [44]. The LRBFM offers an effective approach for performing accurate and efficient numerical simulations of complex PDE models [45–47] across a range of dimensions and domain types.

The article employs a local meshless technique based on Gaussian RBFs to efficiently solve Black-Scholes option models. This approach enables the accurate and efficient computation of solutions for the time-fractional Black-Scholes model by focusing on localized regions rather than relying on a global mesh. The localized RBF method is versatile and can be extended to various fractional Black-Scholes model variants, other financial partial differential equation problems, and situations involving fractional derivatives. This flexibility makes it a powerful tool for addressing complex financial models where traditional methods may struggle to capture intricate behaviors.

Fundamental definitions

The core concept in fractional calculus is fractional derivatives, which extend the traditional notion of integer-

order derivatives to non-integer orders. These derivatives are crucial for modeling complex systems that exhibit memory and hereditary properties, which are not adequately captured by classical calculus. Several fundamental definitions of fractional derivatives are commonly utilized, including the Riemann-Liouville, Caputo, and Atangana-Baleanu derivatives. Each of these definitions has unique characteristics and is suitable for different types of problems, making them essential tools in the study and application of fractional calculus across various scientific and engineering fields. Some foundational definitions that are widely used for fractional derivatives include the following.

Definition 1.1. *The Riemann-Liouville derivative [9, 48]:*

$$\frac{\partial^\alpha P(\overline{\mathbf{y}},t)}{\partial t^\alpha} = \frac{1}{\Gamma(1-\alpha)}\frac{d}{dt}\int_t^T \frac{(P(\overline{\mathbf{y}},\vartheta)-P(\overline{\mathbf{y}},T))}{(\vartheta-t)^\alpha}d\vartheta, \tag{1.3}$$

where $0<\alpha<1$.

Definition 1.2. *Caputo's fractional derivative [49] is a widely used definition of fractional differentiation that extends the concept of integer-order derivatives to non-integer orders. It is particularly valued for its ability to handle initial conditions in a more physically meaningful way compared to other fractional derivatives. The Caputo derivative is defined as:*

$$\frac{\partial^\alpha P(\overline{\mathbf{y}},t)}{\partial t^\alpha} = \frac{1}{\Gamma(1-\alpha)}\int_0^t \frac{\partial P(\overline{\mathbf{y}},\vartheta)}{\partial\vartheta}(t-\vartheta)^{-\alpha}\,d\vartheta, \tag{1.4}$$

where $0<\alpha<1$.

Definition 1.3. *The fractional derivative introduced by Atangana and Baleanu [50]:*

$${}^{ABC}_{a}\frac{\partial^\alpha P(\overline{\mathbf{y}},t)}{\partial t^\alpha} = \frac{B(\alpha)}{1-\alpha}\int_a^t P'(\overline{\mathbf{y}})E_\alpha\left(-\frac{\alpha(t-\overline{\mathbf{y}})^\alpha}{1-\alpha}\right)d\overline{\mathbf{y}}, \tag{1.5}$$

where $0<\alpha<1$.

Definition 1.4. *The fractional derivative as described by He [51]:*

$$\frac{\partial^\alpha P(\overline{\mathbf{y}},t)}{\partial t^\alpha} = \frac{1}{\Gamma(1-\alpha)}\frac{d}{d\overline{\mathbf{y}}}\int_{t_0}^t (t-\vartheta)^{-\alpha}[P_0(\vartheta)-P(\vartheta)], \tag{1.6}$$

where $0<\alpha<1$.

2. Time-discretization techniques within a theoretical framework

First, we outline the basic ideas from functional analysis that are necessary in order to discretize the time variable. These concepts provide the theoretical foundation needed to effectively approximate and analyze the behavior of functions over time, facilitating the application of the proposed numerical methods in solving time-fractional problems.

Foundations of applied functional analysis: An introductory overview

Let $d\overline{\mathbf{y}}$ represent the Lebesgue measure on $\mathbb{R}^2$, and let Ξ be a bounded and open subset of $\mathbb{R}^2$. The space $L^s(\Xi)$ consists of all measurable functions P: $\Xi \longrightarrow \mathbb{R}$, which satisfy:

$$\int_\Xi |P(\overline{\mathbf{y}})|^s d\overline{\mathbf{y}} \le \infty,$$

for a finite value of s. The norm can be used to denote this Banach space as:

$$\|P\|_{L^s(\Xi)} = \left(\int_\Xi |P(\overline{\mathbf{y}})|^s d\overline{\mathbf{y}}\right)^{\frac{1}{s}}.$$

The inner product of the Hilbert space $L^s(\Xi)$ is defined as:

$$(P,U) = \int_\Xi P(\overline{\mathbf{y}})U(\overline{\mathbf{y}})d\overline{\mathbf{y}},$$

utilizing the L^2 norm definition:

$$\|P\|_2 = [(P,P)]^{\frac{1}{2}} = \left[\int_\Xi P(\overline{\mathbf{y}})P(\overline{\mathbf{y}})d\overline{\mathbf{y}}\right]^{\frac{1}{2}}.$$

Furthermore, suppose that in $\mathbb{R}^d$, Ξ is an open domain, with $\gamma = (\zeta_1,\ldots,\zeta_d)$.

$$|\zeta| = \sum_{i=1}^p \zeta_i,$$

denotes a d-tuple of non-negative integers. This leads us to define the following expression:

$$D^\zeta U = \frac{\partial^{|\gamma|}U}{\partial\overline{\mathbf{y}}_1^\zeta\partial\overline{\mathbf{y}}_2^\zeta\cdots\partial\overline{\mathbf{y}}_d^\zeta}.$$

One can obtain:

$$H^1(\Xi) = \left\{ U \in L^2(\Xi), \frac{dU}{d\overline{\mathbf{y}}} \in L^2(\Xi) \right\},$$
$$H_0^1(\Xi) = \left\{ U \in H^1(\Xi),\, U|_{\partial(\Xi)} = 0 \right\},$$
$$H^m(\Xi) = \Big\{ U \in L^2(\Xi), D^\zeta U \in L^2(\Xi) \text{ for all positive integer } |\zeta| \le m \Big\}.$$

In this case, we define an inner product in terms of a Hilbert space.

$$(P, U)_m = \sum_{|\zeta| \le m} \int_\Xi D^\zeta P(\overline{\mathbf{y}}) D^\zeta U(\overline{\mathbf{y}}) d\overline{\mathbf{y}}.$$

This results in the norm:

$$\|U\|_{H^m(\Xi)} = \left(\sum_{|\zeta| \le m} \left\| D^\zeta U \right\|^2_{L^2(\Xi)} \right)^{\frac{1}{2}}.$$

The Sobolev space $X^{1,s}(\mathcal{I})$ is described as

$$X^{1,s}(\mathcal{I}) = U \in L^s(\mathcal{I}), \exists f \in L^S(\mathcal{I}),$$
$$\int_{\mathcal{I}} P\psi' = \int_{\mathcal{I}} f\psi', \forall \psi \in C^1(\mathcal{I}).$$

Moreover, we define the inner product that follows as well as the associated energy norms L^2 and H^1 in this work.

$$\|U\| = (U, U)^{1/2}, \quad \|U\|_1 = (U, U)_1^{1/2}$$

and

$$|U|_1 = \left(\frac{\partial U}{\partial \overline{\mathbf{y}}}, \frac{\partial U}{\partial \overline{\mathbf{y}}} \right)^{1/2},$$

through $L^2(\Xi)$ and $H^1(\Xi)$ inner products:

$$(P, U) = \int P(\overline{\mathbf{y}}) U(\overline{\mathbf{y}}) d\overline{\mathbf{y}}, \quad (P, U)_1 = (P, U) + \left(\frac{\partial P}{\partial \overline{\mathbf{y}}}, \frac{\partial U}{\partial \overline{\mathbf{y}}} \right),$$

respectively.

The time mesh size is given by ($\Delta t = \frac{T}{M}$, and the total number of temporal discretization points M are defined as $t_i = i\Delta t$, where $i \in \mathbb{N}^+$.

Lemma 2.1. *Assume that* $0 < \alpha < 1$ *and* $\eta(t) \in C^2[0, T]$. *Next, it implies that:*

$$\int_0^{t_i} \eta'(\overline{\mathbf{y}}) (t_i - \overline{\mathbf{y}})^{-\alpha} d\overline{\mathbf{y}} = \sum_{s=1}^{i} \frac{\eta(t_s) - \eta(t_{s-1})}{\Delta t},$$
$$\int_{t_{s-1}}^{t_s} (t_i - \overline{\mathbf{y}})^{-\alpha} d\overline{\mathbf{y}} + R^i, \quad 1 \le i \le M$$

and

$$\left| R^i \right| \le \left(\frac{1}{2(1-\alpha)} + \frac{1}{2} \right) \Delta t^{2-\alpha} \max_{0 \le t \le t_i} \left| \eta''(t) \right|.$$

Proof. See Sun et al. [52]. □

Lemma 2.2. *Let* $0 < \alpha < 1$,

$$A_0 = \frac{1}{\Delta t \Gamma(1-\alpha)}$$

and

$$b_p = \frac{\Delta t^{1-\alpha}}{(1-\alpha)} \left[(p+1)^{1-\alpha} - (p)^{1-\alpha} \right],$$

then,

$$\frac{1}{\Gamma(1-\alpha)} \int_0^{t_i} \frac{\eta'(\overline{\mathbf{y}})}{(t_i - \overline{\mathbf{y}})^\alpha} d\overline{\mathbf{y}}$$
$$- A_0 \left[b_0 \eta(t_i) - \sum_{p=1}^{i-1} \left(b_{i-p-1} - b_{i-p} \right) \eta\left(t_p \right) - b_{i-1} \eta(0) \right]$$
$$\le \frac{1}{2\Gamma(1-\alpha)} \left(1 + \frac{1}{(1-\alpha)} \right) \Delta t^{2-\alpha} \max_{0 \le t \le t_i} \left| \eta''(t) \right|.$$

Proof. In accordance directly with Lemma 2.1. □

Lemma 2.3. *Let*

$$b_p = \frac{\Delta t^{1-\alpha}}{(1-\alpha)} \left[(p+1)^{1-\alpha} - (p)^{1-\alpha} \right],$$

where $p = 0, 1, 2, \ldots,$ $0 < \alpha < 1$, *then* $b_0 > b_1 > b_2 > \cdots > b_p \to 0$, *as* $p \to \infty$.

Proof. Details are available in [52]. □

3. Spatial discretization

The proposed LRBFM is formulated within the framework of the differential quadrature method, a robust numerical technique for approximating derivatives in the solution of partial differential equations. This method approximates the derivative of a function at a given point as a weighted sum of the function values at a set of discrete nodes. The integration of RBFs into this framework introduces significant flexibility, enabling the method to effectively manage irregularly spaced nodes and complex geometries. RBFs, including Gaussian, multiquadric, and inverse multiquadric functions, are utilized to construct the weighting coefficients within the proposed method, thereby enhancing both accuracy and stability. Consequently, LRBFM emerges as a versatile and efficient approach for addressing a broad spectrum of problems in computational science and engineering, particularly those involving

complex boundary conditions and multi-dimensional domains.

The LRBFM approximates the spatial derivatives by discretizing them. At the centers $\overline{\mathbf{y}}_\hbar$, the derivatives of $P(\overline{\mathbf{y}}, t)$ are estimated using the local neighborhood around $\overline{\mathbf{y}}_\hbar$, $\{\overline{\mathbf{y}}_{\hbar 1}, \overline{\mathbf{y}}_{\hbar 2}, \overline{\mathbf{y}}_{\hbar 3}, ..., \overline{\mathbf{y}}_{\hbar n_\hbar}\} \subset \{\overline{\mathbf{y}}_1, \overline{\mathbf{y}}_2, \ldots, \overline{\mathbf{y}}_{N^n}\}, n_\hbar \ll N^n$, where $n_\hbar \ll N^n$ and $\hbar = 1, 2, \ldots, N^n$. In 1D, $\overline{\mathbf{y}}$ corresponds to y, while in 2D, $\overline{\mathbf{y}}$ represents (y, z).

Currently in the 1D case:

$$P^{(m)}(y_\hbar) \approx \sum_{k=1}^{n_\hbar} \Lambda_k^{(m)} P(y_{\hbar k}),\ \hbar = 1, 2, \ldots, N. \tag{3.1}$$

By using RBF $\Psi(\|y - y_p\|)$ in (3.1), we get

$$\Psi^{(m)}(\|y_\hbar - y_p\|) = \sum_{k=1}^{n_\hbar} \Lambda_{\hbar k}^{(m)} \Psi(\|y_{\hbar k} - y_p\|),\ p = \hbar 1, \hbar 2, \ldots, \hbar n_\hbar, \tag{3.2}$$

where for Gaussian (GA) RBF $\Psi(\|y_{\hbar k} - y_p\|) = e^{(c\|y_{\hbar k} - y_p\|)^2}$. Matrix form of (3.2) is:

$$\underbrace{\begin{bmatrix} \Psi_{\hbar 1}^{(m)}(y_\hbar) \\ \Psi_{\hbar 2}^{(m)}(y_\hbar) \\ \vdots \\ \Psi_{\hbar n_\hbar}^{(m)}(y_\hbar) \end{bmatrix}}_{\boldsymbol{\Psi}_{n_\hbar}^{(m)}} = \underbrace{\begin{bmatrix} \Psi_{\hbar 1}(y_{\hbar 1}) & \Psi_{\hbar 2}(y_{\hbar 1}) & \cdots & \Psi_{\hbar n_\hbar}(y_{\hbar 1}) \\ \Psi_{\hbar 1}(y_{\hbar 2}) & \Psi_{\hbar 2}(y_{\hbar 2}) & \cdots & \Psi_{\hbar n_\hbar}(y_{\hbar 2}) \\ \vdots & \vdots & \ddots & \vdots \\ \Psi_{\hbar 1}(y\hbar_{n_\hbar}) & \Psi_{\hbar 2}(y_{\hbar n_\hbar}) & \cdots & \Psi_{\hbar n_\hbar}(y\hbar_{n_\hbar}) \end{bmatrix}}_{\mathbf{B}_{n_\hbar}} \underbrace{\begin{bmatrix} \Lambda_{\hbar 1}^{(m)} \\ \Lambda_{\hbar 2}^{(m)} \\ \vdots \\ \Lambda_{\hbar n_\hbar}^{(m)} \end{bmatrix}}_{\boldsymbol{\Lambda}_{n_\hbar}^{(m)}}, \tag{3.3}$$

where

$$\Psi_p(y_k) = \Psi(\|y_k - y_p\|),\ p = \hbar 1, \hbar 2, \ldots, \hbar n_\hbar, \tag{3.4}$$

for each $k = \hbar 1, \hbar 2, \ldots, \hbar n_\hbar$. (3.3) can be written as:

$$\boldsymbol{\Psi}_{n_\hbar}^{(m)} = \mathbf{B}_{n_\hbar} \boldsymbol{\Lambda}_{n_\hbar}^{(m)}, \tag{3.5}$$

$\mathbf{B}_{n_\hbar}$ is guaranteed to be invertible [53]. By using (3.5), we can get:

$$\boldsymbol{\Lambda}_{n_\hbar}^{(m)} = \mathbf{B}_{n_\hbar}^{-1} \boldsymbol{\Psi}_{n_\hbar}^{(m)}. \tag{3.6}$$

From (3.1) and (3.6), we have:

$$P^{(m)}(y_\hbar) = (\boldsymbol{\Lambda}_{n_\hbar}^{(m)})^T \mathbf{P}_{n_\hbar}, \tag{3.7}$$

where

$$\mathbf{P}_{n_\hbar} = [P(y_{\hbar 1}), P(y_{\hbar 2}), \ldots, P(y_{\hbar n_\hbar})]^T. \tag{3.8}$$

For a 2D scenario, approximating the derivatives of $P(y, z, t)$ with respect to y and z as:

$$P_y^{(m)}(y_\hbar, z_\hbar) \approx \sum_{k=1}^{n_\hbar} \beta_k^{(m)} P(y_{\hbar k}, z_{\hbar k}),\ \hbar = 1, 2, \ldots, N^2, \tag{3.9}$$

$$P_z^{(m)}(y_\hbar, z_\hbar) \approx \sum_{k=1}^{n_\hbar} \gamma_k^{(m)} P(y_{\hbar k}, z_{\hbar k}),\ \hbar = 1, 2, \ldots, N^2. \tag{3.10}$$

To determine the corresponding coefficients $\beta_k^{(m)}$ and $\gamma_k^{(m)}$ for $k = 1, 2, \ldots, n_\hbar$, we proceed as follows:

$$\boldsymbol{\beta}_{n_\hbar}^{(m)} = \mathbf{B}_{n_\hbar}^{-1} \boldsymbol{\Phi}_{n_\hbar}^{(m)}, \tag{3.11}$$

$$\boldsymbol{\gamma}_{n_\hbar}^{(m)} = \mathbf{B}_{n_\hbar}^{-1} \boldsymbol{\Phi}_{n_\hbar}^{(m)}. \tag{3.12}$$

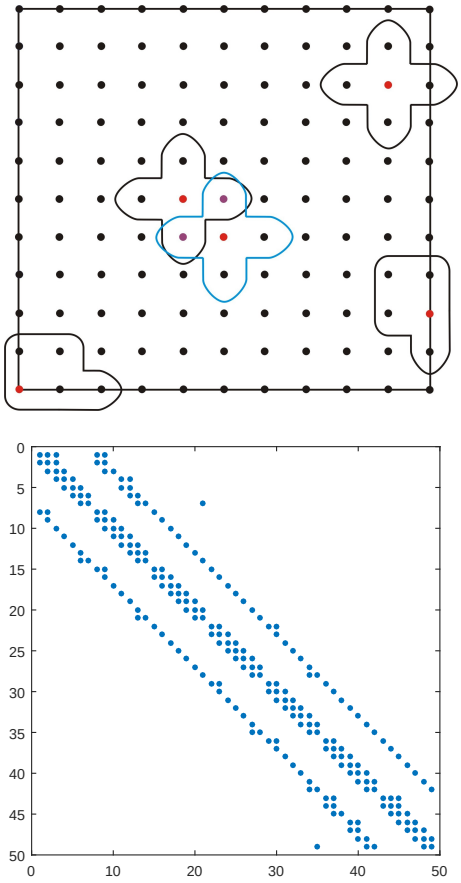

Figure 1. Schematics view (left) and sparsity pattern (right) of the LRBFM in case of 2D for local sub-domain 5.

Local stencils are constructed around each center $\overline{\mathbf{y}}_h$ in two-dimensional geometries, as illustrated in Figure 1 (left). The sparsity pattern for the LRBFM, corresponding to local stencils five, is shown in Figure 1 (right) for the 2D model coefficient matrix. This indicates that the sparse banded matrices generated by the local meshless method can be efficiently solved using sparse matrix solvers.

4. Time discretization

The Caputo fractional time derivative $\frac{\partial^\alpha P(\overline{\mathbf{y}},t)}{\partial t^\alpha}$ for $\alpha \in (0,1)$ is discretized as:

$$\frac{\partial^\alpha P(\overline{\mathbf{y}},t)}{\partial t^\alpha} = \begin{cases} \frac{1}{\Gamma(1-\alpha)} \int_0^t \frac{\partial P(\overline{\mathbf{y}},\vartheta)}{\partial \vartheta} (t-\vartheta)^{-\alpha} \, d\vartheta, & 0 < \alpha < 1, \\ \frac{\partial P(\overline{\mathbf{y}},t)}{\partial t}, & \alpha = 1. \end{cases} \tag{4.1}$$

After approximating the first-order derivative in the time-fractional term using a finite difference technique, we get the following:

$$\frac{\partial^\alpha P(\overline{\mathbf{y}},t_{q+1})}{\partial t^\alpha} = \begin{cases} \frac{\Delta t^{-\alpha}}{\Gamma(2-\alpha)}(P^{q+1}-P^q) \\ +\frac{\Delta t^{-\alpha}}{\Gamma(2-\alpha)} \sum_{p=1}^{q} (P^{q+1-p}-P^{q-p})[(p+1)^{1-\alpha}-p^{1-\alpha}] \\ +R^{p+1}(\overline{\mathbf{z}}), \qquad q \geq 1, \\ \frac{\Delta t^{-\alpha}}{\Gamma(2-\alpha)}(P^1-P^0), \quad q = 0, \end{cases} \tag{4.2}$$

Considering $A_0 = \frac{\Delta t^{-\alpha}}{\Gamma(2-\alpha)}$, $p = 0, 1, \ldots, q$, and $b_p = (p+1)^{1-\alpha} - p^{1-\alpha}$. The equation above can be expressed as:

$$\frac{\partial^\alpha P(\overline{\mathbf{y}},t_{q+1})}{\partial t^\alpha} = \begin{cases} A_0(P^{q+1}-P^q) + A_0 \sum_{p=1}^{q} b_p(P^{q+1-p}-P^{q-p}) \\ +R^{p+1}(\overline{\mathbf{y}}), \qquad q \geq 1, \\ A_0(P^1-P^0), \quad q = 0. \end{cases} \tag{4.3}$$

5. θ-weighted scheme

By employing the θ-weighted method to approximate the model (1.1) in the time domain via (4.3), we derive:

$$\frac{\partial^\alpha P}{\partial t^\alpha} \equiv \mathfrak{L}P, \tag{5.1}$$

now for $q \geq 1$

$$\begin{aligned} &A_0P^{(q+1)} - A_0P^{(q)} + A_0 \sum_{p=1}^{q} b_p(P^{q+1-p} - P^{q-p}) \\ &= \theta\mathfrak{L}P^{(q+1)} + (1-\theta)\mathfrak{L}P^{(q)}, \end{aligned} \tag{5.2}$$

we get:

$$\begin{aligned} P^{(q+1)} = (A_0\mathcal{I} - \theta\mathfrak{L})^{-1} \Big(&(A_0\mathcal{I} + (1-\theta)\mathfrak{L})P^{(q)} \\ &+A_0 \sum_{p=1}^{q} b_p(P^{q+1-p} - P^{q-p}) \Big), \end{aligned} \tag{5.3}$$

in the same way, for $q = 0$

$$P^{(1)} = (A_0\mathcal{I} - \theta\mathfrak{L})^{-1} \left((A_0\mathcal{I} + (1-\theta)\mathfrak{L})P^{(0)} \right), \tag{5.4}$$

After applying the LRBFM (discussed in Section 3), (5.3)–(5.4) lead to:

$$\begin{aligned} P^{(q+1)} = &(A_0\mathcal{I} - \theta\mathcal{L})^{-1} \Big((A_0\mathcal{I} + (1-\theta)\mathcal{L})P^{(q)} \\ &+A_0 \sum_{p=1}^{q} b_p(P^{q+1-p} - P^{q-p}) \Big), \end{aligned} \tag{5.5}$$

$$P^{(1)} = (A_0\mathcal{I} - \theta\mathcal{L})^{-1} \left((A_0\mathcal{I} + (1-\theta)\mathcal{L})P^{(0)} \right), \tag{5.6}$$

where as $\mathcal{I}$ represents the identity matrix, and $\mathcal{L}$ denotes the weights matrix of the differential operator $\mathfrak{L}$. For $\theta = 1$, (5.5)-(5.6) reduce to a totally implicit approach.

6. Stability analysis

The error of Eq (5.6) at the nth time level is defined as $\mathcal{E}^{(n)} = P^{(n)}_{\text{exact}} - P^{(n)}$. This value is chosen to assess the numerical stability of the LRBFM. Therefore, we can express the error $\mathcal{E}^{(n+1)}$ as follows:

$$\mathcal{E}^{(n+1)} = \mathcal{W}\mathcal{E}^{(n)}.$$

The amplification matrix is defined as $\mathcal{W} = (A_0\mathcal{I} - \theta\mathfrak{L})^{-1}((A_0\mathcal{I} + (1-\theta)\mathfrak{L}))$.

The spectral radius of $\mathcal{W}$, denoted as $\rho(\mathcal{W})$, must satisfy $\rho(\mathcal{W}) \leq 1$ to ensure numerical stability. The θ-weighted scheme is formulated as follows under this condition:

$$\left| \frac{1 + (1-\theta)\Delta t\lambda}{1 - \theta\Delta t\lambda} \right| \leq 1, \tag{6.1}$$

where the eigenvalue of the matrix Ω is λ. Consequently, the inequality (6.1) simplifies to:

For $\theta = 1$, the scheme is fully implicit, and the stability condition is given by:

$$\left|\frac{1}{1-\Delta t\lambda}\right| \leq 1. \tag{6.2}$$

For $\theta = 0.5$, the scheme corresponds to the Crank-Nicolson method, and the stability condition is:

$$\left|\frac{1+0.5\Delta t\lambda}{1-0.5\Delta t\lambda}\right| \leq 1. \tag{6.3}$$

For $\theta = 0$, the scheme is explicit, and the stability condition simplifies to:

$$\left|\frac{1+\Delta t\lambda}{1}\right| \leq 1. \tag{6.4}$$

In the explicit case, this implies that:

$$\Delta t \leq \frac{-2}{\lambda} \quad \text{and} \quad \lambda \leq 0.$$

The following is the format of the inequalities (6.2)–(6.4) for the complex eigenvalue $\lambda = x_1 + ix_2$, where x_1, x_2 are any real numbers:

For the full implicit scheme:

$$\left|\frac{1}{1-\Delta t(x_1+ix_2)}\right| \leq 1,$$

implying

$$\frac{1}{\sqrt{1+\Delta t^2x_1^2+\Delta t^2x_2^2-2\Delta tx_1}} \leq 1. \tag{6.5}$$

For the Crank-Nicolson scheme:

$$\left|\frac{1+0.5\Delta t(x_1+ix_2)}{1-0.5\Delta t(x_1+ix_2)}\right| \leq 1,$$

implying

$$\sqrt{\frac{1+0.25\Delta t^2x_1^2+0.25\Delta t^2x_2^2+\Delta tx_1}{1+0.25\Delta t^2x_1^2+0.25\Delta t^2x_2^2-\Delta ta}} \leq 1. \tag{6.6}$$

Similarly, for the explicit scheme:

$$\left|\frac{1+\Delta t(x_1+ix_2)}{1}\right| \leq 1,$$

implying

$$\Delta t \leq \frac{-2x_1}{x_1^2+x_2^2}, \tag{6.7}$$

as long as in each of the inequalities (6.2)–(6.7), $Re(\lambda) \leq 0$.

The Crank-Nicolson and implicit schemes exhibit unconditional stability, whereas the explicit scheme demonstrates conditional stability, as indicated by the previously discussed inequalities. In contrast to traditional methods, the number of nodes N and the shape parameter c affect the stability of meshless procedures. The condition number in the global meshless approach of the collocation matrix is particularly sensitive to the value of the shape parameter c. Variations in c can quickly lead to an ill-conditioned system [44]. In contrast, the proposed LRBFM does not exhibit these complications.

7. Numerical results

We validate that the suggested LRBFM for time-fractional partial differential equations (PDEs) is applicable and accurate. This validation involves applying LRBFM to two-asset American options and digital options. We assess the method's effectiveness in handling the complexities of time-fractional dynamics and ensure that it provides reliable and accurate numerical solutions for these types of PDEs. The successful application of LRBFM to these option models demonstrates its robustness and precision in addressing time-fractional option pricing challenges. The accuracy of the problems is measured using maximum error norm.

In the numerical computation for the American option, the spatial domain [0,4] is utilized, with parameters $\sigma_1 = 0.2$, $\sigma_2 = 0.3$, $D_1 = 0.05$, $D_2 = 0.01$ $\rho = 0.03$, $r = 0.2$, $E = 1$, along with a time step $\Delta t = 0.005$. For the digital call option, the spatial domain [0,2] is employed, using the same parameters $\sigma_1 = 0.2$, $\sigma_2 = 0.2$, $D_1 = 0$, $D_2 = 0$ $\rho = 0.3$, $r = 0.05$, $E = 0.5$, and time step $\Delta t = 0.005$.

Test problem 7.1. *The Black-Scholes model [5], as a free boundary value problem, represents the two-asset American put option and is detailed in [54, 55].*

$$\frac{\partial^\alpha P}{\partial t^\alpha} = \frac{1}{2}\sigma_1^2y^2\frac{\partial^2P}{\partial y^2} + \frac{1}{2}\sigma_2^2z^2\frac{\partial^2P}{\partial z^2} + \frac{1}{2}\rho\sigma_1\sigma_2yz\frac{\partial^2P}{\partial y\partial z} + (r-D_1)y\frac{\partial P}{\partial y} + (r-D_2)z\frac{\partial P}{\partial z} - rP, \quad y,z \geq 0,\ t \in [0,T]. \tag{7.1}$$

The space variables y and z denote the prices of the underlying assets. The following variables are shown, in

order: σ_i, D_i, ρ_{ij}, r, T, and P; they correspond to the volatility of the ith asset, dividend paid by the ith asset, correlation between the ith and jth assets, risk-free interest rate, expiry time, and the option value.

Converting the Eq (7.1) *into a fixed domain model by employing the penalty term approach [56, 57].*

$$\begin{aligned}\frac{\partial^\alpha P}{\partial t^\alpha} &= \frac{1}{2}\sigma_1^2 y^2\frac{\partial^2 P}{\partial y^2} + \frac{1}{2}\sigma_2^2 z^2\frac{\partial^2 P}{\partial z^2} + \frac{1}{2}\rho\sigma_1\sigma_2 yz\frac{\partial^2 P}{\partial y\partial z}\\ &\quad + (r-D_1)y\frac{\partial P}{\partial y} + (r-D_2)z\frac{\partial P}{\partial z} - rP + \frac{\mu C}{P+\mu-q}\\ &\equiv \mathfrak{L}P(y,z,t), \quad y,z\geq 0,\ t\in[0,T],\end{aligned} \tag{7.2}$$

where $0 \leq \mu \ll 1$, $q = E - (a_1 y + a_2 z)$, *and* $C \geq rE$.
The initial and boundary conditions are given as:

$$P(y,z,0) = E - (a_1 y + a_2 z), \quad y,z \geq 0. \tag{7.3}$$

$$\begin{aligned} P(y,0,t) &= g_1(y), \quad y\geq 0,\ t\in[0,T],\\ P(0,z,t) &= g_2(z), \quad z\geq 0,\ t\in[0,T],\\ \lim_{z\to\infty} P(y,z,t) &= 0, \quad y\geq 0,\ t\in[0,T],\\ \lim_{y\to\infty} P(y,z,t) &= 0, \quad z\geq 0,\ t\in[0,T].\end{aligned} \tag{7.4}$$

To determine the boundary functions g_1 and g_2 for the relevant single-asset American put option problem., the constants a_1 and a_2 are utilized. However, explicit analytical solutions for g_1 and g_2 are generally not available, as they are solutions to single-asset American option pricing problems. Numerical approximations are employed to address these issues, as discussed in [58, 59]. The focus here is on single-asset American option pricing models incorporating fractional Black-Scholes operators, which correspond to the boundary problems g_1 and g_2.

Due to the lack of an exact solution for Eq (7.2)*, Table 1 presents numerical results for different values of N and α obtained using the double mesh method. Figures 2 and 3 show the numerical solutions for the two-asset American option at $\alpha = 1$ and $\alpha = 0.5, 0.7$ with $N = 30$ and $t = 1$. To illustrate the effect of α on the option value, Figure 4 provides cross-sections of Test Problem 7.1 at $y = z$ for various $\alpha = 1, 0.9, 0.7, 0.5, 0.3$. Additionally, Figures 5 and 6 present a comparison of the risk-free interest rate r for $\alpha = 1$ and $\alpha = 0.5$.*

Table 1. Comparison at various uniform nodes and α of maximum error norm for Test Problem 7.1.

α	$N = 64$	$N = 128$	$N = 256$	$N = 512$	$N = 1024$
0.3	2.4907×10^{-01}	3.7890×10^{-02}	9.0462×10^{-03}	4.9451×10^{-03}	2.1246×10^{-03}
0.5	3.8314×10^{-02}	8.5819×10^{-03}	5.6414×10^{-03}	3.1752×10^{-03}	8.9332×10^{-04}
0.7	4.4825×10^{-02}	5.7281×10^{-03}	2.6812×10^{-03}	6.9155×10^{-04}	4.9486×10^{-04}
0.9	4.0178×10^{-02}	3.0131×10^{-03}	8.1047×10^{-04}	5.7831×10^{-04}	3.0342×10^{-04}

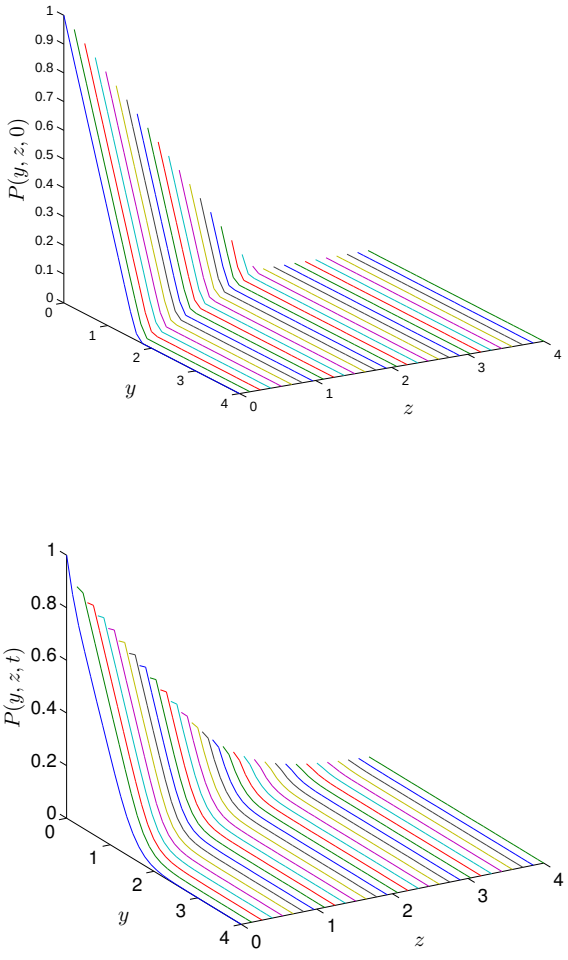

Figure 2. Payoff (left) and $\alpha = 1$ (right) using $N = 30$ and $T = 1$ for the American option problem 7.1.

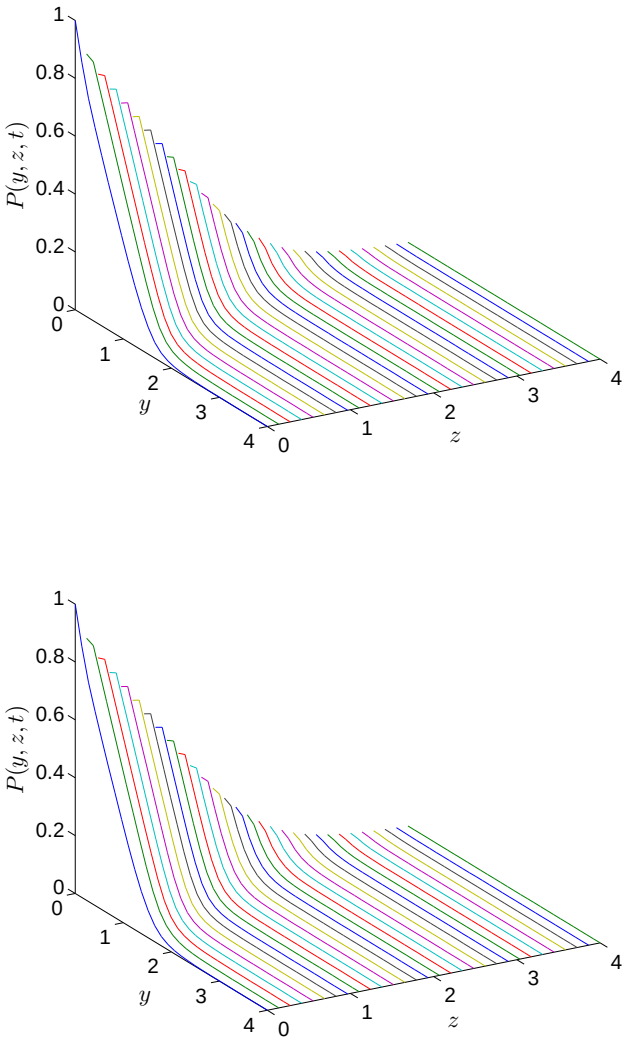

Figure 3. Numerical solution at $\alpha = 0.5$ (left) and $\alpha = 0.7$ (right) using $N = 30$ and $T = 1$ for the American option problem 7.1.

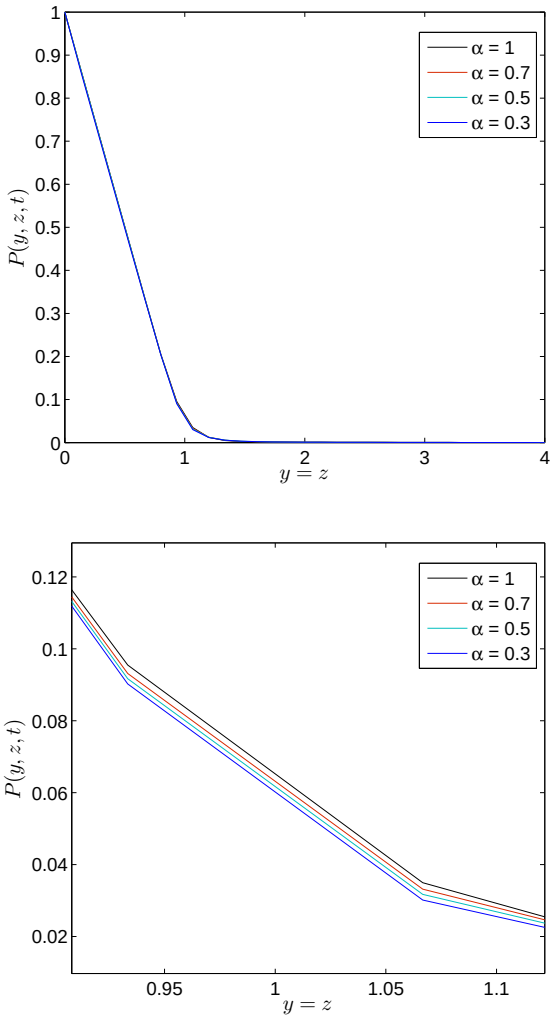

Figure 4. Numerical solution at final time using various α (left) and its close view (right) for the Test Problem 7.1.

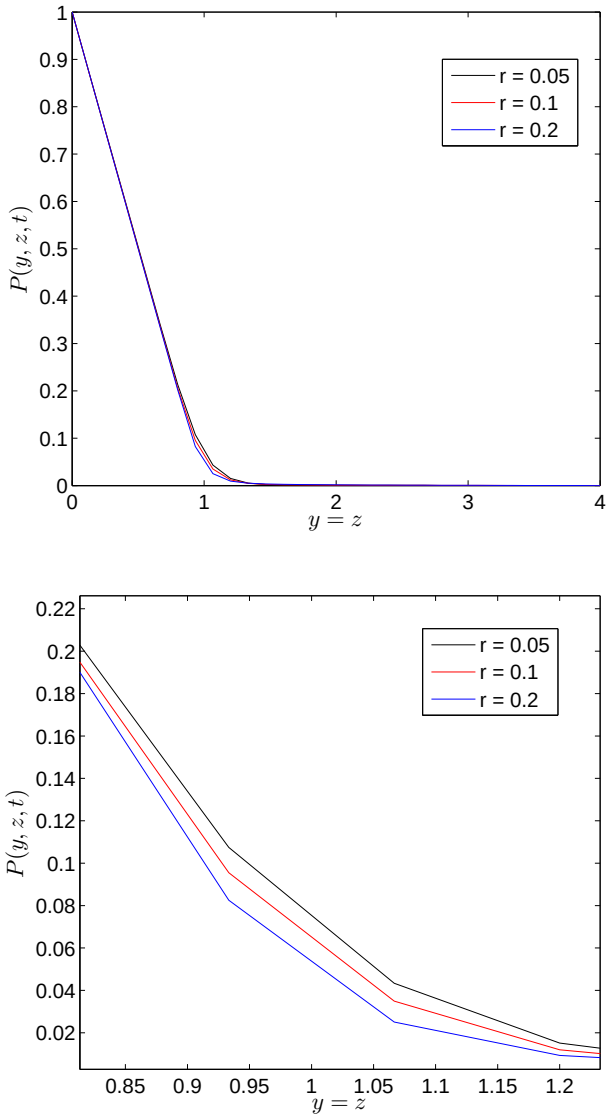

Figure 5. Numerical solutions using various r and $T = 1$ of the two-asset American option at $\alpha = 1$ (left) and its close view (right) for the Test Problem 7.1.

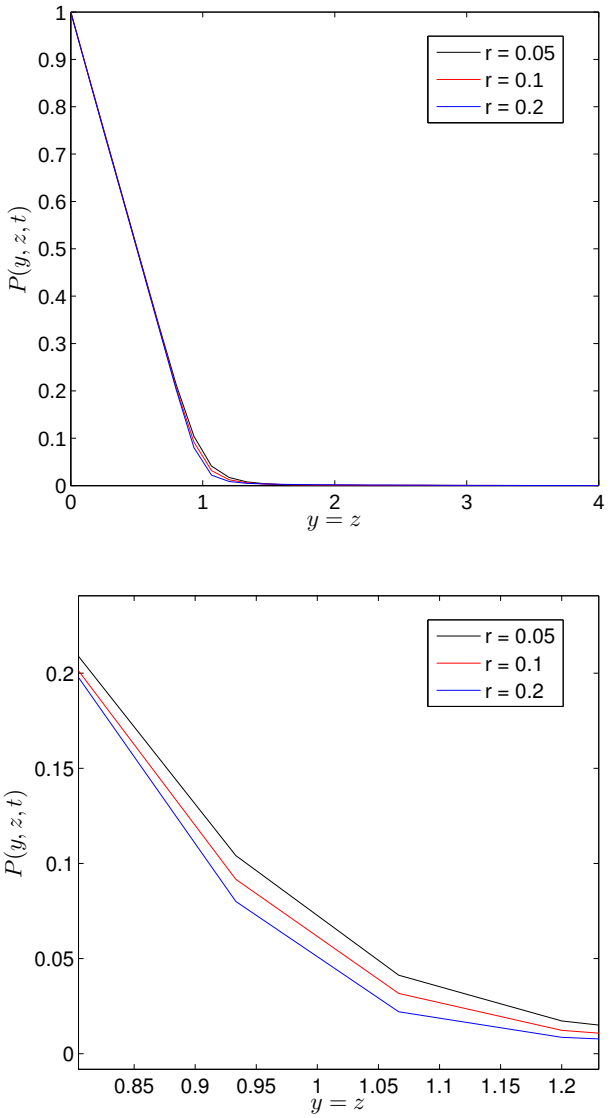

Figure 6. Numerical solutions using various r and $T = 1$ of the two-asset American option at $\alpha = 0.5$ (left) and its close view (right) for the Test Problem 7.1.

Test problem 7.2. *Consider the following time fractional digital call/cash or nothing call option [60]*

$$\frac{\partial^\alpha P}{\partial t^\alpha} = \frac{1}{2}\sigma_1^2 y^2 \frac{\partial^2 P}{\partial y^2} + \frac{1}{2}\sigma_2^2 z^2 \frac{\partial^2 P}{\partial z^2} + \frac{1}{2}\rho\sigma_1\sigma_2 yz \frac{\partial^2 P}{\partial yz} + (r - D_1)y\frac{\partial P}{\partial y} + (r - D_2)z\frac{\partial P}{\partial z} - rP. \tag{7.5}$$

The asset prices are denoted by y and z with an initial

condition

$$P(y,z,0) = \begin{cases} 1 & \text{if } \max\{y,z\} \geq E, \\ 0 & \text{if otherwise.} \end{cases} \tag{7.6}$$

In the absence of an exact analytical solution for Eq (7.2)*, Table 2 provides numerical results for varying values of N and α, obtained through the double mesh method. Figures 7 and 8 depict the numerical solutions for the two-asset digital option at* $\alpha = 1$ *as well as* $\alpha = 0.5$ *and* 0.7*, with* $N = 30$ *and* $t = 1$*. To elucidate the influence of α on the option value, Figure 9 presents cross-sectional views of Test Problem 7.2 at* $y = z$ *for* $\alpha = 1, 0.9, 0.7, 0.5,$ *and* 0.3*. Furthermore, Figure 10 offers a comparative analysis of the risk-free interest rate r for* $\alpha = 1$ *and* $\alpha = 0.5$*.*

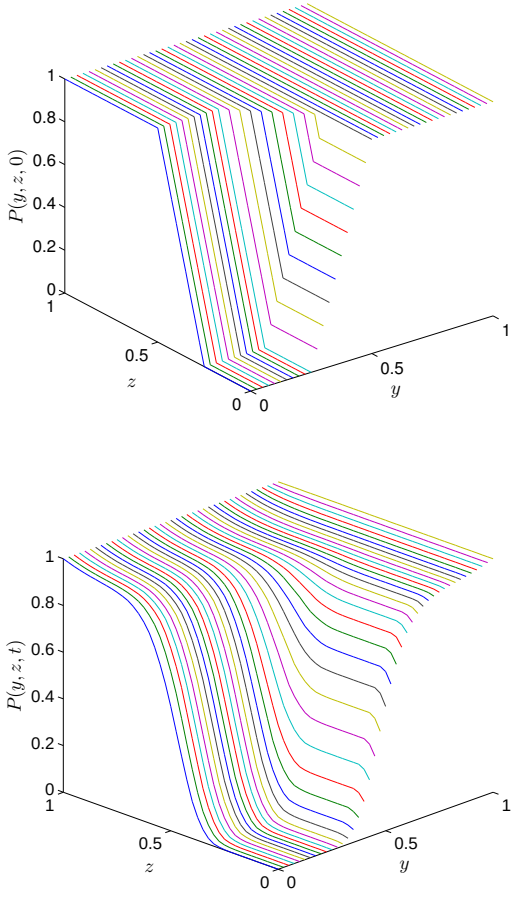

Figure 7. Payoff (left) and $\alpha = 1$ (right) using $N = 30$ and $T = 1$ for the digital option problem 7.2.

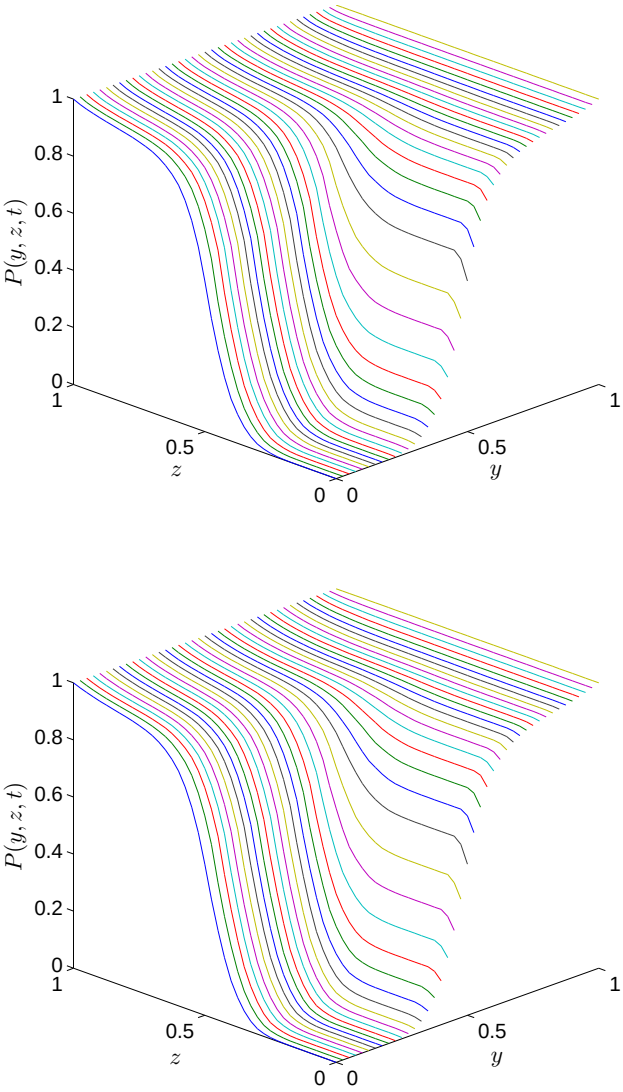

Figure 8. Numerical solution at $\alpha = 0.5$ (left) and $\alpha = 0.7$ (right) using $N = 30$ and $T = 1$ for the digital option problem 7.2.

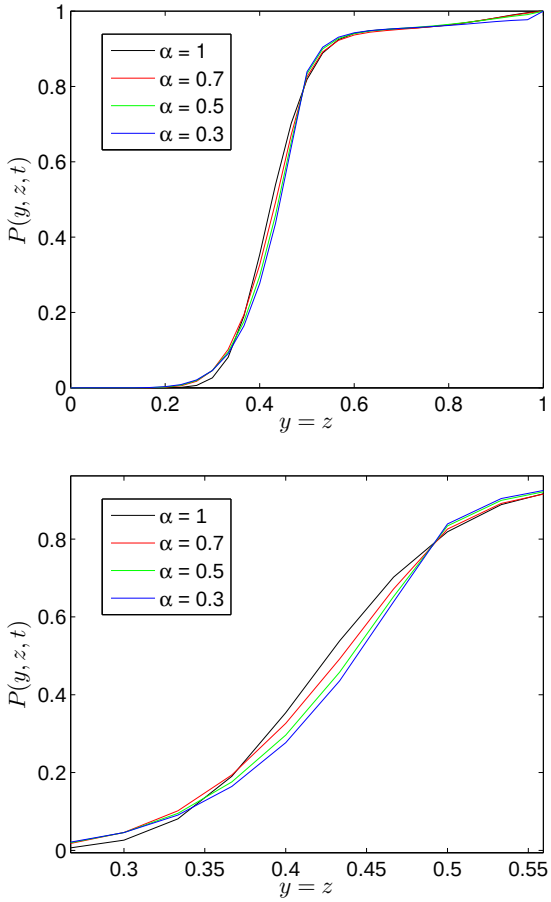

Figure 9. Numerical solution at final time using various α (left) and its close view (right) for the Test Problem 7.2.

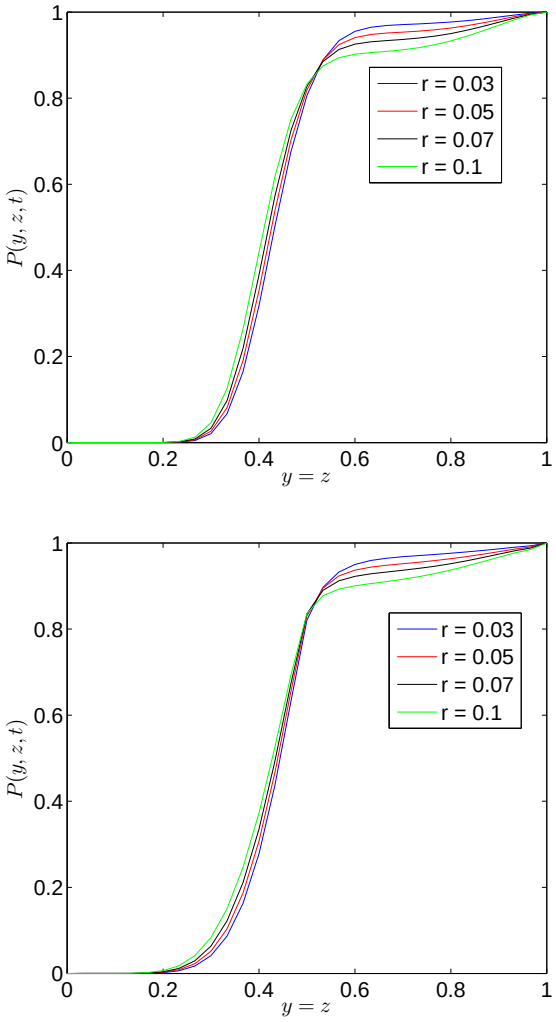

Figure 10. Numerical solutions using various r and $T = 1$ of the two-asset digital option at $\alpha = 1$ (left) and $\alpha = 0.5$ (right) for the Test Problem 7.2.

Table 2. Comparison at various uniform nodes and α of maximum error norm for Test Problem 7.2.

α	$N = 64$	$N = 128$	$N = 256$	$N = 512$	$N = 1024$
0.3	7.9326× 10^{-02}	7.0623× 10^{-02}	3.1657× 10^{-02}	6.9737× 10^{-03}	3.8249× 10^{-03}
0.5	6.9430× 10^{-02}	3.2201× 10^{-02}	7.8476× 10^{-03}	5.5901× 10^{-03}	6.2329× 10^{-04}
0.7	6.8213× 10^{-02}	2.2746× 10^{-02}	6.8803× 10^{-03}	5.2594× $\times 10^{-03}$	5.7329× 10^{-04}
0.9	7.5288× 10^{-03}	4.9102× 10^{-03}	3.0262× 10^{-03}	8.9453× 10^{-04}	6.0216× 10^{-04}

8. Conclusions

In this study, the local radial basis function collocation method (LRBFM) has been effectively applied to obtain approximate results for the time-fractional Black-Scholes model (TFBSM) for both two-asset American and digital options. To assess the advantages of the TFBSM over the conventional Black-Scholes model for call and put options, we conducted numerical simulations across different values of α. The TFBSM demonstrates superior accuracy in modeling phenomena such as large movements or jumps compared to the traditional Black-Scholes approach. Our findings indicate that the LRBFM accurately discretizes spatial derivatives and handles complexities such as interest rates, underscoring its robustness and applicability to multi-asset options. The rigorous evaluation of the proposed approach using L_∞ error norms, along with validation through the double mesh technique, affirmed the accuracy and efficiency of the method. The numerical outcomes for various option pricing models within the framework of fractional partial differential equations confirm the robustness and practicality of the LRBFM.

Use of Generative-AI tools declaration

The authors declare that they have not used artificial intelligence tools in the creation of this article.

Conflict of interest

Authors declare no conflicts of interest in this paper.

References

1. S. B. Chen, H. Jahanshahi, O. A. Abba, J. E. Solís-Pérez, S. Bekiros, J. F. Gómez-Aguilar, et al., The effect of market confidence on a financial system from the perspective of fractional calculus: Numerical investigation and circuit realization, *Chaos, Soliton. Fract.*, **140** (2020), 110223. https://doi.org/10.1016/j.chaos.2020.110223
2. P. Ma, A. Najafi, J. F. Gomez-Aguilar, Sub mixed fractional Brownian motion and its application to finance, *Chaos, Soliton. Fract.*, **184** (2024), 114968. https://doi.org/10.1016/j.chaos.2024.114968
3. J. Wu, J. F. Gomez-Aguilar, R. Taleghani, Portfolio optimization under the uncertain financial model, *Comput. Econ.*, 2024, 1–22. https://doi.org/10.1007/s10614-024-10727-w
4. J. P. Aguilar, J. Korbel, N. Pesci, On the quantitative properties of some market models involving fractional derivatives, *Mathematics*, **9** (2021), 3198. https://doi.org/10.3390/math9243198
5. F. Black, M. Scholes, The pricing of options and corporate liabilities, *J. Polit. Econ.*, **81** (1973), 637–654. https://doi.org/10.1086/260062
6. P. Carr, L. Wu, The finite moment log stable process and option pricing, *J. Finance*, **58** (2003), 753–777. https://doi.org/10.1111/1540-6261.00544
7. A. I. Alaje, M. O. Olayiwola, K. A. Adedokun, J. A. Adedeji, A. O. Oladapo, Y. O. Akeem, The modified homotopy perturbation method and its application to the dynamics of price evolution in Caputo-fractional order Black Scholes model, *Beni-Suef Univ. J. Basic Appl. Sci.*, **12** (2023), 93. https://doi.org/10.1186/s43088-023-00433-1
8. S. N. Ogunyebi, S. E. Fadugba, T. O. Ogunlade, K. J. Adebayo, B. T. Babalola, O. Faweya, et al., Direct solution of the Black-Scholes PDE models with non-integer order, *J. Phys. Conf. Ser.*, **2199** (2022), 012003. https://doi.org/10.1088/1742-6596/2199/1/012003
9. G. Jumarie, Derivation and solutions of some fractional Black-Scholes equations in coarse-grained space and time. application to merton's optimal portfolio, *Comput. Math. Appl.*, **59** (2010), 1142–1164. https://doi.org/10.1016/j.camwa.2009.05.015
10. J. Korbel, Y. Luchko, Modeling of financial processes with a space-time fractional diffusion equation of varying order, *Fract. Calc. Appl. Anal.*, **19** (2016), 1414–1433. https://doi.org/10.1515/fca-2016-0073
11. A. Farhadi, M. Salehi, G. H. Erjaee, A new version of Black-Scholes equation presented by time-fractional derivative, *Iran J. Sci. Technol. Trans. Sci.*, **42** (2018), 2159–2166. https://doi.org/10.1007/s40995-017-0244-7

12. A. Cartea, D. del Castillo-Negrete, Fractional diffusion models of option prices in markets with jumps, *Phys. A: Stat. Mech. Appl.*, **374** (2007), 749–763. https://doi.org/10.1016/j.physa.2006.08.071

13. Q. Li, Y. Zhou, X. Zhao, X. Ge, Fractional order stochastic differential equation with application in European option pricing, *Discrete Dyn. Nat. Soc.*, **2014** (2014), 621895. https://doi.org/10.1155/2014/621895

14. W. Chen, X. Xu, S. P. Zhu, A predictor–corrector approach for pricing American options under the finite moment log-stable model, *Appl. Numer. Math.*, **97** (2015), 15–29. https://doi.org/10.1016/j.apnum.2015.06.004

15. W. Chen, S. Wang, A penalty method for a fractional order parabolic variational inequality governing American put option valuation, *Comput. Math. Appl.*, **67** (2014) 77–90. https://doi.org/10.1016/j.camwa.2013.10.007

16. G. Colldeforns-Papiol, L. Ortiz-Gracia, C. W. Oosterlee, Two-dimensional Shannon wavelet inverse Fourier technique for pricing European options, *Appl. Numer. Math.*, **117** (2017), 115–138. https://doi.org/10.1016/j.apnum.2017.03.002

17. M. J. Ruijter, C. W. Oosterlee, Two-dimensional Fourier cosine series expansion method for pricing financial options, *SIAM J. Sci. Comput.*, **34** (2012), B642–B671. https://doi.org/10.1137/120862053

18. Q. J. Meng, D. Ding, An efficient pricing method for rainbow options based on two-dimensional modified sine–sine series expansions, *Int. J. Comput. Math.*, **90** (2013), 1096–1113. https://doi.org/10.1080/00207160.2012.749349

19. W. Wang, X. Chen, D. Ding, S. L. Lei, Circulant preconditioning technique for barrier options pricing under fractional diffusion models, *Int. J. Comput. Math.*, **92** (2015), 2596–2614. https://doi.org/10.1080/00207160.2015.1077948

20. X. Chen, W. Wang, D. Ding, S. L. Lei, A fast preconditioned policy iteration method for solving the tempered fractional HJB equation governing American options valuation, *Comput. Math. Appl.*, **73** (2017), 1932–1944. https://doi.org/10.1016/j.camwa.2017.02.040

21. S. L. Lei, W. Wang, X. Chen, D. Ding, A fast preconditioned penalty method for American options pricing under regime-switching tempered fractional diffusion models, *J. Sci. Comput.*, **75** (2018), 1633–1655. https://doi.org/10.1007/s10915-017-0602-9

22. S. Kim, D. Jeong, C. Lee, J. Kim, Finite difference method for the multi-asset Black–Scholes equations, *Mathematics*, **8** (2020), 391. https://doi.org/10.3390/math8030391

23. D. Černá, K. Fiňková, Option pricing under multifactor Black–Scholes model using orthogonal spline wavelets, *Math. Comput. Simul.*, **220** (2024), 309–340. https://doi.org/10.1016/j.matcom.2024.01.020

24. J. Choi, Sum of all Black–Scholes–Merton models: an efficient pricing method for spread, basket, and Asian options, *J. Futures Markets*, **38** (2018), 627–644. https://doi.org/10.1002/fut.21909

25. C. Bayer, C. B. Hammouda, A. Papapantoleon, M. Samet, R. Tempone, Quasi-Monte Carlo for efficient fourier pricing of multi-asset options, *arXiv Preprint*, 2024. https://doi.org/10.48550/arXiv.2403.02832

26. W. Chen, S. Wang, A 2nd-order FDM for a 2D fractional Black-Scholes equation, In: I. Dimov, I. Faragó, L. Vulkov, *Numerical analysis and its applications*, NAA 2016, Lecture Notes in Computer Science, Springer, Cham., **10187** (2017), 46–57. https://doi.org/10.1007/978-3-319-57099-0_5

27. W. Chen, S. Wang, A power penalty method for a 2D fractional partial differential linear complementarity problem governing two-asset American option pricing, *Appl. Math. Comput.*, **305** (2017), 174–187. https://doi.org/10.1016/j.amc.2017.01.069

28. L. Mohan, A. Prakash, Stability and numerical analysis of the generalised time-fractional Cattaneo model for heat conduction in porous media, *Eur. Phys. J. Plus*, **138** (2023), 1–28. https://doi.org/10.1140/epjp/s13360-023-03765-0

29. K. S. Chaudhary, N. Kumar, Fractional order fast terminal sliding mode control scheme for tracking control of robot manipulators, *ISA Trans.*, **142** (2023), 57–69. https://doi.org/10.1016/j.isatra.2023.08.008

30. N. Kumar, K. S Chaudhary, Motion control of underactuated Cart-Double-Pendulum system Via fractional-order sliding mode controller, In: R. Kumar, A. K. Verma, O. P. Verma, T. Wadehra, *Soft computing: theories and applications*, SoCTA 2023, Lecture Notes in Networks and Systems, Springer, Singapore, **970** (2023), 155–165. https://doi.org/10.1007/978-981-97-2031-6_14

31. I. Ahmad, A. A. Bakar, R. Jan, S. Yussof, Dynamic behaviors of a modified computer virus model: insights into parameters and network attributes, *Alex. Eng. J.*, **103** (2024), 266–277. https://doi.org/10.1016/j.aej.2024.06.009

32. A. A. Khan, M. Ahsan, I. Ahmad, M. Alwuthaynani, Enhanced resolution in solving first-order nonlinear differential equations with integral condition: a high-order wavelet approach, *Eur. Phys. J. Spec. Top.*, 2024, 1–14. https://doi.org/10.1140/epjs/s11734-024-01254-8

33. A. Prakash, L. Mohan, Two efficient techniques for analysis and simulation of time-fractional Tricomi equation, *Sādhanā*, **49** (2024), 1–13. https://doi.org/10.1007/s12046-024-02482-3

34. I. Ali, I. Ahmad, Applications of the nonlinear Klein/Sinh-Gordon equations in modern physics: a numerical study, *Math. Model. Control*, **4** (2024), 361–373. https://doi.org/10.3934/mmc.2024029

35. J. F. Li, I. Ahmad, H. Ahmad, D. Shah, Y. M. Chu, P. Thounthong, et al., Numerical solution of two-term time-fractional PDE models arising in mathematical physics using local meshless method, *Open Phys.*, **18** (2020), 1063–1072. https://doi.org/10.1515/phys-2020-0222

36. F. Wang, I. Ahmad, H. Ahmad, M. D. Alsulami, K. S. Alimgeer, C. Cesarano, et al., Meshless method based on RBFs for solving three-dimensional multi-term time fractional PDEs arising in engineering phenomenons, *J. King Saud Univ.-Sci.*, **33** (2021), 101604. https://doi.org/10.1016/j.jksus.2021.101604

37. F. Wang, M. N. Khan, I. Ahmad, H. Ahmad, H. Abu-Zinadah, Y. M. Chu, Numerical solution of traveling waves in chemical kinetics: time-fractional Fishers equations, *Fractals*, **30** (2022), 2240051. https://doi.org/10.1142/S0218348X22400515

38. I. Ahmad, M. Ahsan, I. Hussain, P. Kumam, W. Kumam, Numerical simulation of PDEs by local meshless differential quadrature collocation method, *Symmetry*, **11** (2019), 394. https://doi.org/10.3390/sym11030394

39. I. Ahmad, A. O. Alshammari, R. Jan, N. N. A. Razak, S. A. Idris, An efficient numerical solution of a multi-dimensional two-term fractional order PDE via a hybrid methodology: the Caputo–Lucas–Fibonacci approach with strang splitting, *Fractal Fract.*, **8** (2024), 364. https://doi.org/10.3390/fractalfract8060364

40. M. N. Khan, I. Ahmad, M. Shakeel, R. Jan, Fractional calculus analysis: investigating Drinfeld-Sokolov-Wilson system and Harry Dym equations via meshless procedures, *Math. Model. Control*, **4** (2024), 86–100. https://doi.org/10.3934/mmc.2024008

41. M. N. Khan, I. Ahmad, A. Akgül, H. Ahmad, P. Thounthong, Numerical solution of time-fractional coupled Korteweg–de Vries and Klein–Gordon equations by local meshless method, *Pramana*, **95** (2021), 1–13. https://doi.org/10.1007/s12043-020-02025-5

42. I. Ahmad, M. Ahsan, Z. Din, A. Masood, P. Kumam, An efficient local formulation for time–dependent PDEs, *Mathematics*, **7** (2019), 216. https://doi.org/10.3390/math7030216

43. G. Yao, Siraj-ul-Islam, B. Sarler, A comparative study of global and local meshless methods for diffusion-reaction equation, *Comput. Model. Eng. Sci.*, **59** (2010), 127–154. https://doi.org/10.3970/cmes.2010.059.127

44. Siraj-ul-Islam, I. Ahmad, A comparative analysis of local meshless formulation for multi-asset option models, *Eng. Anal. Bound. Elem.*, **65** (2016), 159–176. https://doi.org/10.1016/j.enganabound.2015.12.020

45. L. Mohan, A. Prakash, An efficient technique for solving fractional diffusion equations arising in oil pollution via natural transform, *Waves Random Complex Media*, 2023, 1–22. https://doi.org/10.1080/17455030.2023.2273323

46. L. Mohan, A. Prakash, Stability and numerical analysis of fractional BBM-Burger equation and fractional diffusion-wave equation with Caputo derivative, *Opt. Quant. Electron.*, **56** (2024), 26. https://doi.org/10.1007/s11082-023-05608-9

47. A. Prakash, L. Mohan, Application of Caputo fractional operator to analyse the fractional model of Brain Tumour via modified technique, *Int. J. Appl. Comput. Math.*, **9** (2023), 117. https://doi.org/10.1007/s40819-023-01591-7

48. G. Jumarie, Stock exchange fractional dynamics defined as fractional exponential growth driven by (usual) Gaussian white noise. Application to fractional Black-Scholes equations, *Insur.: Math. Econ.*, **42** (2008), 271–287. https://doi.org/10.1016/j.insmatheco.2007.03.001

49. M. Caputo, Linear models of dissipation whose Q is almost frequency independent-II, *Geophys. J. Int.*, **13** (1967), 529–539. https://doi.org/10.1111/j.1365-246X.1967.tb02303.x

50. A. Atangana, D. Baleanu, New fractional derivatives with non-local and nonsingular kernel theory and application to heat transfer model, *Therm. Sci.*, **20** (2016), 763–769. https://doi.org/10.2298/TSCI160111018A

51. J. H. He, Z. B. Li, Q. L. Wang, A new fractional derivative and its application to explanation of polar bear hairs, *J. King Saud. Univ.-Sci.*, **28** (2016), 190–192. https://doi.org/10.1016/j.jksus.2015.03.004

52. Z. Z. Sun, X. Wu, A fully discrete difference scheme for a diffusion-wave system, *Appl. Numer. Math.*, **56** (2006), 193–209. https://doi.org/10.1016/j.apnum.2005.03.003

53. S. A. Sarra, A local radial basis function method for advection–diffusion–reaction equations on complexly shaped domains, *Appl. Math. Comput.*, **218** (2012), 9853–9865. https://doi.org/10.1016/j.amc.2012.03.062

54. A. Q. M. Khaliq, D. A. Voss, K. Kazmi, Adaptive θ-methods for pricing American options, *J. Comput. Appl. Math.*, **222** (2008), 210–227. https://doi.org/10.1016/j.cam.2007.10.035

55. M. K. Kadalbajooa, A. Kumar, L. P. Tripathia, Application of local radial basis function based finite difference method for American option problems, *Int. J. Comput. Math.*, **92** (2015), 1608–1624. https://doi.org/10.1080/00207160.2014.950571

56. B. F. Nielsen, O. Skavhaug, A. Tveito, Penalty and front-fixing methods for the numerical solution of American option problems, *J. Comput. Finance*, **5** (2002), 69–97. https://doi.org/10.21314/JCF.2002.084

57. G. E. Fasshauer, A. Q. M. Khaliq, D. A. Voss, Using meshfree approximation for multi-asset American option problems, *J. Chin. Inst. Eng.*, **27** (2004), 563–571. https://doi.org/10.1080/02533839.2004.9670904

58. C. S. Huang, C. H. Hung, S. Wang, A fitted finite volume method for the valuation of options on assets with stochastic volatilities, *Computing*, **77** (2006), 297–320. https://doi.org/10.1007/s00607-006-0164-4

59. C. S. Huang, C. H. Hung, S. Wang, On convergence of a fitted finite-volume method for the valuation of options on assets with stochastic volatilities, *IMA J. Numer. Anal.*, **30** (2010), 1101–1120. https://doi.org/10.1093/imanum/drp016

60. Z. Cen, J. Huang, A. Xu, A. Le, Numerical approximation of a time-fractional Black–Scholes equation, *Comput. Math. Appl.*, **75** (2018), 2874–2887. https://doi.org/10.1016/j.camwa.2018.01.016

AIMS Press